JACS Au
AN OPEN ACCESS JOURNAL OF THE AMERICAN CHEMICAL SOCIETY

pubs.acs.org/jacsau
Letter

Hydroxyl Radical–π Interaction in a Single Crystal

Mohit Kulshrestha, Abhijit Nandy, Shibdas Banerjee,* Srinu Tothadi,* C. N. Ramachandran,* and Kalyan K. Sadhu*

Cite This: *JACS Au* 2025, 5, 61–66

Read Online

ACCESS | Metrics & More | Article Recommendations | Supporting Information

ABSTRACT: Numerous attempts for organic radical stability mostly entail steric hindrance, spin-delocalization, supramolecular interaction with the host, $\pi-\pi$ interactions, and hydrogen bonding. To date, there is no report of single crystals containing a hydroxyl radical ($^{\bullet}$OH). In this work, we have stabilized $^{\bullet}$OH in the crystal, which has been obtained from the filtrate after separating the precipitate of the chromenopyridine radical (DCP(2)$^{\bullet}$) from the reaction mixture. DCP(2)$^{\bullet}$ abstracts a hydrogen atom from dissolved water in the ethanolic filtrate to grow the single crystal containing DCPH(2) and $^{\bullet}$OH in the asymmetric unit. The crystal packing and computational studies suggest that $\pi-^{\bullet}$OH and $^{\bullet}$OH···N hydrogen-bonding interactions are responsible for stabilizing $^{\bullet}$OH. The presence of $^{\bullet}$OH has been further confirmed by mass analysis with the 2,2,6,6-tetramethylpiperidin-1-yl)oxyl (TEMPO) adduct. Solid-state electron paramagnetic resonance (EPR), solution state nitroblue tetrazolium (NBT) assay, and spin trapping with 5,5-dimethyl-1-pyrroline *N*-oxide (DMPO) in the presence of super oxide dismutase suggest $^{\bullet}$OH formation in the single crystal.

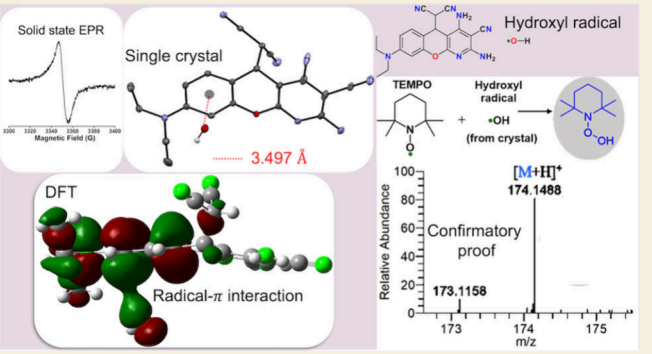

KEYWORDS: *carbon-centered radical, hydroxyl radical, single crystal, spin trapping, radical–π interaction*

Organic radicals are transient in nature due to their high energy, and they undergo dimerization, hydrogen abstraction, or disproportionation. These short-lived species find utility in material sciences due to their astounding electronic and magnetic properties, yet their short lifetime presents challenges.[1−3] To increase the lifetime of the radicals, steric requirements in the synthesis have been designed.[4−6] In addition to the introduction of a sterically demanding group, supramolecular interactions with cage molecules have been explored to stabilize radicals.[7−10] Intermolecular interactions like $\pi-\pi$ stacking between aromatic rings and van der Waals forces are known to stabilize the radicals in molecular aggregates.[11−14] Hydrogen bonding has also been reported to stabilize a biologically relevant flavin radical and other organic radical anions.[15,16] The stabilities of semiquinone and amino acid radicals have been enhanced due to encapsulation within a metalloenzyme, a peptide, and protein folds.[17−20]

In biological systems, radicals are being produced every moment during cellular processes, out of which reactive oxygen species (ROS), mainly the superoxide anion ($O_2^{\bullet-}$) and $^{\bullet}$OH, are of utmost importance. Above optimal concentration, ROS are responsible for the oxidation of DNA and lipids, causing tissue damage, oxidative stress, aging, and diseases like cancer, Alzheimer's, and Parkinson's.[21−25] The ROS are now being utilized for waste treatment by oxidizing the waste and also for cancer therapeutics.[26,27] In addition to the biological activities of $^{\bullet}$OH, it can participate in organic synthesis, modification of proteins, and polymerization and has very recently demonstrated to accelerate zeolite crystallization.[28] To date, the synthesis of $^{\bullet}$OH has been achieved via applying pulse radiolysis, γ-irradiation on crystalline ice at very low temperature, the Haber–Weiss reaction, the Fenton reaction, and electrochemical processes.[29−32]

Despite extensive chemical research, the stability of $^{\bullet}$OH remains a challenge due to its short lifespan ($\sim 10^{-9}$ s) and its reliance on fluorophores for detection. One electron reduction potential of hydroxyl radical is 2.31 V, which makes it a strong oxidizing agent and makes it unstable.[33] Recently, a uranyl peroxide cluster has been reported to stabilize $^{\bullet}$OH, but without any crystal structure.[34] To the best of our knowledge, to date there is no report on capturing and stabilizing $^{\bullet}$OH in a crystal. In this work, we successfully crystallize $^{\bullet}$OH oxygen (Scheme 1). $^{\bullet}$OH has been stabilized in the crystal by exploiting DCPH(2) $\pi-^{\bullet}$OH and $^{\bullet}$OH···N hydrogen-bonding interactions.[35]

Received: November 21, 2024
Revised: December 30, 2024
Accepted: January 2, 2025
Published: January 9, 2025

Scheme 1. Oxygen-Mediated Syntheses of (a) Previously Reported and (b) Newly Synthesized Chromenopyridine Radicals and the Generation of •OH in a Single Crystal

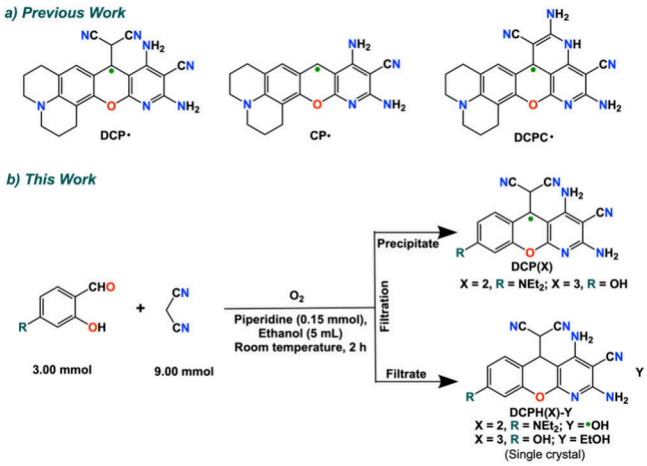

In our recent work, we reported julolidine-based chromenopyridine derivatized radicals DCP•, CP•, and DCPC•, where we obtained DCPC• crystals from the reaction in DMSO.[36] The DMSO filtrate contained a superoxide radical as a product via oxygen-based radical formation. However, we could not isolate or stabilize the superoxide radical during crystallization of DCPC•. Taking this forward as an inspiration to stabilize and crystallize ROS in crystal, we have synthesized the other two DCP• derivatives, DCP(2)• and DCP(3)•, using 4-diethylamino salicylaldehyde and 2,4-dihydroxybenzaldehyde, respectively (Scheme 1).

We performed the reaction between salicylaldehyde derivatives with malononitrile in the presence of a piperidine base. After 2 h of reaction at room temperature, the radical precipitates were separated. The filtrate was kept for crystallization and crystals of DCPH(2) and DCPH(3) were obtained (Scheme 1). Interestingly, DCPH(2) crystallizes along with •OH, whereas the crystal of DCPH(3) has ethanol (EtOH) as a solvent. The solid precipitates that had been obtained from the reaction mixtures showed EPR spectra with a g value of 2.003 for both DCP(2)• and DCP(3)• (Figures S1 and S2) at 100 K. In the solid-state, visible region absorption shows peaks at 420 and 525 nm for DCP(2)• (Figure S3) and at 465 and 495 nm for DCP(3)• (Figure S4). The HRMS data for both DCP(2)• and DCP(3)• show molecular weight peaks at 372.1565 and 317.0785, respectively (Figures S5 and S6). These two radicals show the diamagnetic DCPH(2) or DCPH(3) NMR in DMSO-d_6 (Figures S7−S10) after abstracting hydrogen, like our previous case with julolidine-based DCP•.[36]

The slow evaporation of solvent from the filtrate, after separating the DCP(2)• precipitate, produces orange-colored crystals of DCPH(2)•OH (Figure 1). DCPH(2)•OH crystallizes in a triclinic unit cell, $P\bar{1}$ space group, where an asymmetric unit contains one molecule of DCPH(2), and •OH has 0.75 occupancy. The single crystal study shows that DCPH(2) has a bent shape with two intersecting planes intersecting with a dihedral angle of 14.51° (Figure S11a). The bond lengths (Figure S11b) and bond angles (Figure S11c) around C6 confirm sp^3 hybridization of the same atom along with a $CH(CN)_2$ pendant. The C6−C18 bond (1.588(3) Å) elongates due to the steric and electrostatic repulsion between

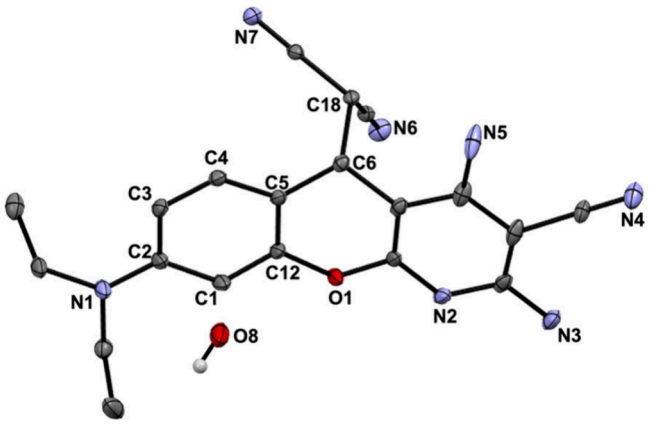

Figure 1. Asymmetric unit of DCPH(2)•OH with 30% thermal ellipsoids probability (H atoms of DCPH(2) have been omitted for clarity).

the overhead nitrile group of dicyanomethyl appendage and middle ring. Computationally predicted DCP• contains a sp^2 hybridized carbon atom, and the overall structure is planar, along with the $CH(CN)^2$ pendant.[36]

Although DCPH(2) is diamagnetic, the crystals are EPR active in the solid state (Figure 2), implying that the positive

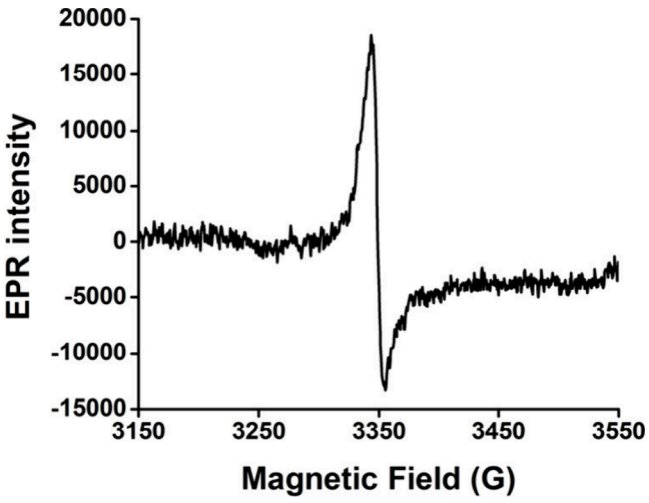

Figure 2. Solid-state EPR at 300 K of DCPH(2)•OH.

signal might be due to the presence of the oxygen-based radical present in the asymmetric unit. The difference Fourier map of DCPH(2)•OH shows only one highest electron density (Q1) peak near the O8 atom (Figure S12). It corresponds to a single hydrogen attached to the atomic position of O8. The presence of only one free oxygen atom (O8) in the asymmetric unit also rules out the possibility of superoxide or peroxide among the ROS in the crystal. However, the limitation of single crystal data with a hydrogen atom is that they cannot confirm the •OH radical unambiguously. Crystal packing geometry suggests weak interactions between the layered structures of DCPH(2) (Figure S13). The minimum distance of N2 to C21 between the two nearest π rings is 3.388(3) Å.

We further planned to directly capture the •OH present in the crystal using a radical trapping agent, namely, TEMPO in dimethylformamide. The DCPH(2)•OH crystal was added to it, followed by overnight incubation at room temperature. The

https://doi.org/10.1021/jacsau.4c01115
JACS Au 2025, 5, 61−66

solution was diluted in acetonitrile for spraying onto a mass spectrometer equipped with a custom-built electrospray source. The mass spectrum recorded from this spray exhibited an ion signal at m/z 174.1488 (Figure 3a), which was

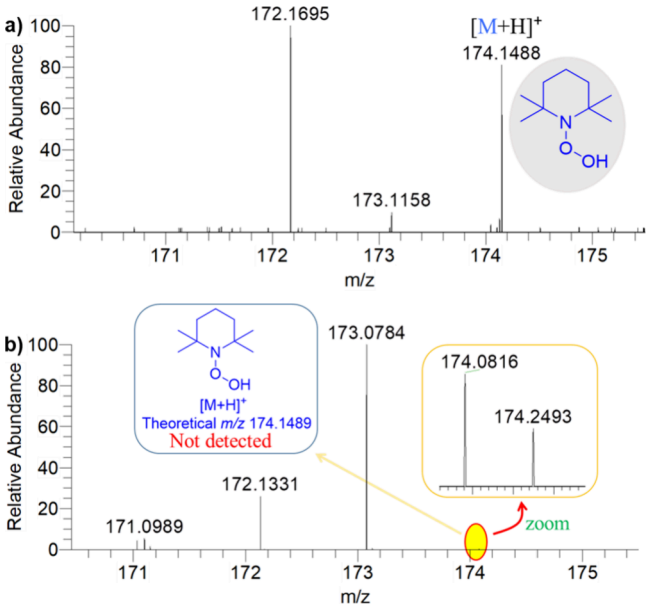

Figure 3. ESI-MS spectra showing the (a) capture of •OH present in the crystal by TEMPO and (b) the absence of the •OH in the control experiment. The unassigned signals do not form the basis of the TEMPO reaction.

attributed to the •OH adduct of TEMPO. The analogous experiment with TEMPO, but without using the crystal, exhibited no ion signal of this species (Figure 3b) in the control experiment, indicating the crystal as the source of •OH. Moreover, it is important to mention that this •OH did not appear from the sprayed organic aerosols, as manifested by the control experiment.[37,38] However, TEMPO did not form an adduct with other bulky organic radicals, probably for steric reasons.

In the case of DCP(3)• precipitate, similar filtrate results are obtained in yellow crystals of DCPH(3).EtOH, where the asymmetric unit contains one molecule of both DCPH(3) and ethanol (Figure S14). DCPH(3).EtOH crystallizes in a monoclinic unit cell, the $P2_1/c$ space group. Similar to the previous case, DCPH(3) is also nonplanar with a dihedral angle of 15.15°. In addition, the bond lengths and bond angles around C6 in DCPH(3) have been found to be in line with tetrahedral geometry. The diamagnetic DCPH(3).EtOH crystals are reflected in the EPR silent behavior (Figure S15).

To understand the elemental conditions[39] of C, N, and O in the crystal, XPS has been performed for DCPH(2)•OH (Figure S16). The XPS spectra for C 1*s* showed three peaks at 282.3, 284.8, and 287.3 eV. The peak at 284.8 eV is responsible for C—C, C═C, and C—H.[40] C═N and C≡N contribute to the peak at 287.3 eV.[41] The peak at 282.3 eV has unusual low binding energy compared to organic compounds, indicating an interaction of the π-cloud of the aromatic ring with •OH. The peak for nitrogen at 397.2 eV is for the pyridine-N, and the deviation from the position is possibly due to substitution around it.[40] The latter peak of N 1s at 399.7 eV is due to the pyridine-amine and nitrile group present in DCPH(2).[42,43] Further, the spectrum for O 1*s* shows two peaks positioned at 531.3 and 533.8 eV for C—O—C and •OH, respectively.[40,44]

To confirm the presence of •OH as ROS, a NBT assay was performed.[45] The absorbance of a solution containing dissolved DCPH(2)•OH and DCPH(3).EtOH crystals in NBT solution produced a broad hump at 570 nm with a tail extended to 700 nm due to formazan selectively forming with DCPH(2)•OH (Figure S17). In addition, DMPO was prepared in DMSO, and the DCPH(2)•OH crystals were directly dissolved in the same solution. The distinct four-peak signal in solution state EPR at 300 K (Figure S18) confirmed the presence of •OH in the crystal.[46] Further, to confirm •OH vs O^{2-} among the ROS, EPR was done in the presence of superoxide dismutase (Figure 4a). The positive signal in the

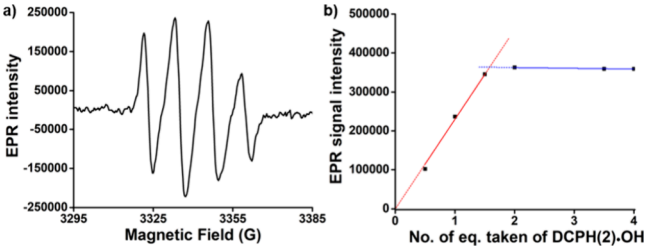

Figure 4. (a) EPR spectrum of DCPH(2)•OH taken in the presence of superoxide dismutase and DMPO, and (b) DMPO titration spectra showing the peak intensity at 3333 G with varying the concentration of DCPH(2)•OH against a constant concentration of DMPO.

presence of the enzyme ruled out the possibility of superoxide as ROS. The variable concentration of the crystal solution was used in EPR titration (Figure S19) with respect to DMPO to determine the equivalent of •OH in the solution. The intersecting straight lines plot suggested the presence of 0.63 equiv of •OH per DCPH(2) molecule (Figures 4b and S19).

Spin quantification has been performed by solid-state magnetism and compared with well-known radical TEMPO. From the $1/\chi$ vs T plot in the solid-state, the crystal has shown a 42% spin quantification at 300 K with respect to $S = 1/2$ spin (Figure S20). At a temperature <220 K, the $1/\chi$ vs T plot shows a deviation from Curie—Weiss behavior. For the $S = 1/2$ spin, the $1/\chi$ vs T plot (Figure S20) and M vs H plot (Figure S21) at 100 K show a spin quantification ~12%. Solution state spin quantification through EPR has been compared with DMPO via the Fenton reaction at 300 K. The calibrated EPR plot in the solution state suggests 25% of spin quantification (Figure S22). The less amount of spin quantification in these two experiments suggests the poor stability of the •OH in the solution state.

Supramolecular interactions[47,48] in the crystal are important factors for the overall stability of •OH. The crystal packing of DCPH(2)•OH suggests that weak interactions, such as hydrogen bonding and radical—π interactions, are responsible for capturing and stabilizing •OH in crystals. The crystal structure shows that •OH has a supramolecular interaction with three molecules of DCPH(2) (Figure 5). The amine hydrogen of one DCPH(2) molecule acts as a hydrogen bond donor to facilitate hydrogen bonding with the •OH. The N3···O8 distance is 2.950(3) Å and the N3—H3A---O8 angle is 160.91(2)°. These distance and angle parameters are well within the limit of Tyr-Asn or Ser-Asn hydrogen bonding N—H···O interactions.[49] The N atom in the nitrile group is disordered over N4 and N8 in DCPH(2). The N4 atom of the

https://doi.org/10.1021/jacsau.4c01115
JACS Au 2025, 5, 61−66

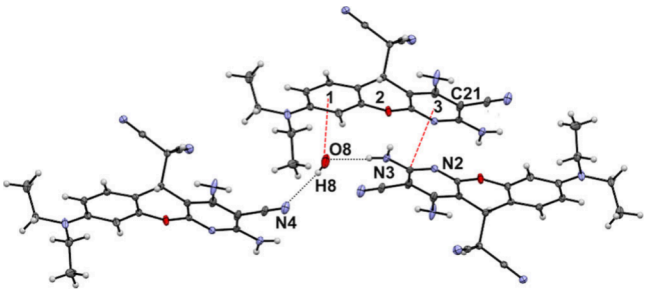

Figure 5. Important intermolecular interactions (---) with rings and hydrogen bonding interactions (···) between •OH and DCPH(2).

second DCPH(2) molecule participates in hydrogen bonding with •OH having a N4···O8 bond distance of 3.115(1) Å and a N4−H8−O8 angle of 164.94(4)°. In addition, the distance between the O8 atom and centroid of the aromatic ring with substituted NEt_2 is 3.497 Å. The above interactions stabilize the hydroxyl radical in the crystal lattice.

To validate the experimental observations, we carried out dispersion-corrected density functional theoretical calculations of DCPH(2)•OH at the B3LYP-D3/6-311G** level, implemented in the Gaussian 09 suite of programs.[50] The calculations were carried out using the coordinates obtained from the crystal structure without further optimization. The interaction of •OH with three units of adjacent DCPH(2) was considered. The natural bond orbital (NBO) analysis confirms the presence of two strong hydrogen bond interactions between •OH and the two units of DCPH(2). In one of these hydrogen bonds, •OH acts as a hydrogen bond donor with one of the DCPH(2) molecules and the other as a hydrogen bond acceptor. The NBO analysis also revealed the hybridization of the oxygen atom of the hydroxyl radical as sp^2 and a weak interaction between the p orbital of the •OH species with the third DCPH(2) unit (Figure 6a). The similar

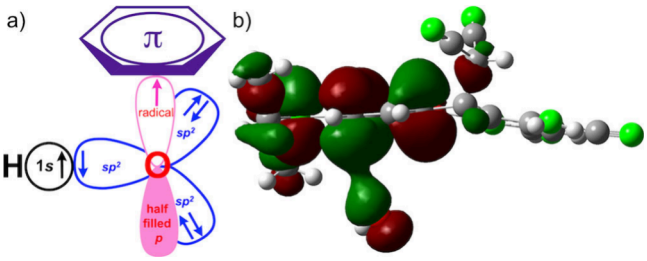

Figure 6. (a) Schematic representation of the electrons of oxygen in three sp^2 and one p orbitals for a favorable radical−π interaction, and (b) a molecular orbital diagram of the asymmetric unit of DCPH(2)•OH with the β-SOMO orbital showing the radical−π interaction between the half-filled p orbital of the oxygen of •OH with the π-cloud of the aromatic ring of DCPH(2).

changes in hybridization were reported for triarylphosphine radical cations.[51] To know more about the radical−π interaction, we carried out molecular orbital analysis of the fragment containing the above DCPH(2)•OH in its doublet state. The relevant molecular orbital depicting the interaction between •OH species with the third unit of DCPH(2) is provided in Figure 6b, showing the interaction of the unhybridized p orbital of the oxygen atom of the hydroxyl radical with the DCPH(2) molecule.

It is known that the total density of states of a complex system and the partial density of states due to the fragments provide information about the interaction between the units.[52] To infer the interaction between the fragments, we calculated the total density of states (TDOS) of the system along with the partial density of states (PDOS) of the fragments using the program Multiwfn.[53] The above density of states (Figure S23) confirms the weak interaction between the DCPH(2) and •OH species. Further, the atomic charges of various atoms of the molecule and its fragments are also calculated (Table S2). The analysis revealed the accumulation of a slight negative charge on the OH moiety, in contrast to the slight positive charge of the DCPH(2) unit, suggesting the interaction between the two units, in agreement with the earlier findings.

Thermogravimetric analysis of DCPH(2)•OH confirms a slow weight loss up to 160 °C due to •OH and a sharp weight loss at 160 °C due to the removal of the nitrile functional group (Figure S24). Similar studies with DCPH(3).EtOH show a ∼20% weight loss at 200 °C due to removal of ethanol and a nitrile group (Figure S25). The infrared studies of DCPH(2)•OH show an additional peak at 3420 cm^{-1} in comparison to DCP(2)• (Figure S26) due to the presence of •OH. The origin of the •OH during crystallization is due to a reversed hydrogen atom shift from the already present water in ethanol for crystallization (Scheme 2). Although the hydrogen

Scheme 2. Reaction between DCP• and Water to Form DCPH(2)•OH and Its Reversible Reaction while Drying

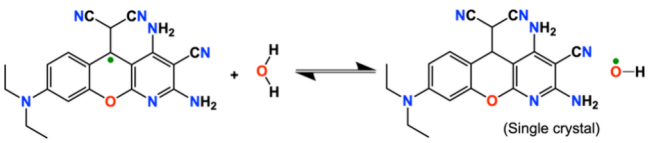

atom shift from water to a single molecule of DCP(2)• is thermodynamically challenging, the stability of the •OH within crystal packing has been achieved by three molecules of DCPH(2) through hydrogen bonding and radical−π interactions (Figure 5).

To check the activity of the hydroxyl radical in glutathione oxidation, we have treated the freshly prepared solution of the crystal with the glutathione-based hydrogels from our recent report.[54] The hydrogels, which are remarkably stable in the presence of H_2O_2, have been converted to sols. The activity of this •OH has been found to be greater in comparison to H_2O_2.

In summary, we have captured •OH in crystals along with the DCPH(2) molecule. The •OH has been stabilized using crystal packing and the nonbonding interactions between DCPH(2) and •OH. The •OH formation has been further investigated with solid-state EPR, solution state NBT assay, DMPO-based EPR, and TEMPO-based mass analysis. We are currently working on the reactivity of •OH in organic reactions.

■ ASSOCIATED CONTENT

Supporting Information

The Supporting Information is available free of charge at https://pubs.acs.org/doi/10.1021/jacsau.4c01115.

Experimental procedures; Compound characterization data; NMR and EPR spectra (PDF)

https://doi.org/10.1021/jacsau.4c01115
JACS Au 2025, 5, 61−66

Accession Codes

CCDC 2351833-2351834 contains the supplementary crystallographic data for this paper. These data can be obtained free of charge via www.ccdc.cam.ac.uk/data_request/cif, by emailing data_request@ccdc.cam.ac.uk, or by contacting The Cambridge Crystallographic Data Centre, 12 Union Road, Cambridge CB2 1EZ, U.K.; fax: +44 1223336033.

AUTHOR INFORMATION

Corresponding Authors

Shibdas Banerjee − *Department of Chemistry, Indian Institute of Science Education and Research Tirupati, Tirupati 517507 Andhra Pradesh, India;* orcid.org/0000-0002-3424-8157; Email: shibdas@iisertirupati.ac.in

Srinu Tothadi − *Analytical and Environmental Sciences Division and Centralized Instrumentation Facility, CSIR-Central Salt and Marine Chemicals Research Institute, Bhavnagar 364002, India*; Email: srinut@csmcri.res.in

C. N. Ramachandran − *Department of Chemistry, Indian Institute of Technology Roorkee, Roorkee 247667 Uttarakhand, India;* orcid.org/0000-0003-2331-5374; Email: ramcn@cy.iitr.ac.in

Kalyan K. Sadhu − *Department of Chemistry, Indian Institute of Technology Roorkee, Roorkee 247667 Uttarakhand, India;* orcid.org/0000-0001-5891-951X; Email: sadhu@cy.iitr.ac.in

Authors

Mohit Kulshrestha − *Department of Chemistry, Indian Institute of Technology Roorkee, Roorkee 247667 Uttarakhand, India;* orcid.org/0009-0005-8774-3230

Abhijit Nandy − *Department of Chemistry, Indian Institute of Science Education and Research Tirupati, Tirupati 517507 Andhra Pradesh, India*

Complete contact information is available at: https://pubs.acs.org/10.1021/jacsau.4c01115

Author Contributions

K.K.S. conceived the idea. M.K. performed the syntheses and characterization of all the experiments except the single crystal of DCPH(2)$^{\bullet}$OH and ESI-MS. A.N. performed the ESI-related experiments. S.B. provided the experimental facility and provided guidance. S.T. solved the single crystal of DCPH(2)$^{\bullet}$OH. C.N.R. performed the DFT calculations. All authors discussed the results and participated in the manuscript writing.

Notes

The authors declare no competing financial interest.

ACKNOWLEDGMENTS

K.K.S. acknowledges the SERB-DST Grant (CRG/2023/001415) for research funding. Authors thank DST-FIST India (SR/FST/CS-II/2018/72(C)) for the 500 MHz NMR and single crystal X-ray diffractometer support. S.T. thanks SERB for the Start-up Research Grant (SRG/2023/000209), and AESD&CIF (MLP0072) and CSIR-CSMCRI for the infrastructure. The authors acknowledge the learned reviewers for their insightful suggestions to improve the quality of the work.

REFERENCES

(1) Ratera, I.; Veciana, J. Playing with organic radicals as building blocks for functional molecular materials. *Chem. Soc. Rev.* **2012**, *41*, 303−349.

(2) Chen, Z. X.; Li, Y.; Huang, F. Persistent and Stable Organic Radicals: Design, Synthesis, and Applications. *Chem.* **2021**, *7*, 288−332.

(3) Mizuno, A.; Matsuoka, R.; Mibu, T.; Kusamoto, T. Luminescent Radicals. *Chem. Rev.* **2024**, *124*, 1034−1121.

(4) Gomberg, M. An instance of trivalent Carbon: Triphenylmethyl. *J. Am. Chem. Soc.* **1900**, *22*, 757−771.

(5) Veciana, J.; Carilla, J.; Miravitlles, C.; Molins, E. Free radicals as clathrate hosts: crystal and molecular structure of 1:1 perchlorotriphenylmethyl radical−benzene. *J. Chem. Soc., Chem. Commun.* **1987**, *11*, 812−814.

(6) Zhang, D.; Cai, M.; Zhang, Y.; Zhang, D.; Duan, L. Sterically shielded blue thermally activated delayed fluorescence emitters with improved efficiency and stability. *Mater. Horiz.* **2016**, *3*, 145−151.

(7) Cai, K.; Zhang, L.; Astumian, R. D.; Stoddart, J. F. Radical-pairing-induced molecular assembly and motion. *Nat. Rev. Chem.* **2021**, *5*, 447−465.

(8) Wang, H.; Xue, K.-F.; Yang, Y.; Hu, H.; Xu, J.-F.; Zhang, X. In Situ Hypoxia-Induced Supramolecular Perylene Diimide Radical Anions in Tumors for Photothermal Therapy with Improved Specificity. *J. Am. Chem. Soc.* **2022**, *144*, 2360−2367.

(9) Jia, F.; Schröder, H. V.; Yang, L.-P.; von Essen, C.; Sobottka, S.; Sarkar, B.; Rissanen, K.; Jiang, W.; Schalley, C. A. Redox-Responsive Host-Guest Chemistry of a Flexible Cage with Naphthalene Walls. *J. Am. Chem. Soc.* **2020**, *142*, 3306−3310.

(10) Hasegawa, S.; Meichsner, S. L.; Holstein, J. J.; Baksi, A.; Kasanmascheff, M.; Clever, G. H. Long-Lived C_{60} Radical Anion Stabilized Inside an Electron-Deficient Coordination Cage. *J. Am. Chem. Soc.* **2021**, *143*, 9718−9723.

(11) Busseron, E.; Cid, J.-J.; Wolf, A.; Du, G.; Moulin, E.; Fuks, G.; Maaloum, M.; Polavarapu, P.; Ruff, A.; Saur, A. K.; Ludwigs, S.; Giuseppone, N. Light-controlled morphologies of self-assembled triarylamine−fullerene conjugates. *ACS Nano* **2015**, *9*, 2760−2772.

(12) Picini, F.; Schneider, S.; Gavat, O.; Vargas Jentzsch, A.; Tan, J.; Maaloum, M.; Strub, J.-M.; Tokunaga, S.; Lehn, J. M.; Moulin, E.; Giuseppone, N. Supramolecular polymerization of triarylamine-based macrocycles into electroactive nanotubes. *J. Am. Chem. Soc.* **2021**, *143*, 6498−6504.

(13) Wang, X.; Zhang, H.; Liu, H.; Xu, G.; Lai, W.; Zhang, Y.; Ni, X.; Xie, S.; Tang, B. Z.; Zeng, Z. Photoelectromagnetic responsive adaptive porous frameworks through dynamic covalent chemistry of tetraarylethylene-backboned aryldicyanomethyl radicals. *Angew. Chem., Int. Ed.* **2023**, *62*, 202301719.

(14) Hou, B.; Li, K.; He, H.; Hu, J.; Xu, Z.; Xiang, Q.; Wang, P.; Chen, X.; Sun, Z. Stable crystalline nanohoop radical and its self-association promoted by van der Waals interactions. *Angew. Chem., Int. Ed.* **2023**, *62*, No. e202301046.

(15) Breinlinger, E.; Niemz, A.; Rotello, V. M. Model systems for flavoenzyme activity. Stabilization of the flavin radical anion through specific hydrogen bond interactions. *J. Am. Chem. Soc.* **1995**, *117*, 5379−5380.

(16) Benson, C. R.; Fatila, E. M.; Lee, S.; Marzo, M. G.; Pink, M.; Mills, M. B.; Preuss, K. E.; Flood, A. H. Extreme stabilization and redox switching of organic anions and radical anions by large-cavity, CH hydrogen-bonding cyanostar macrocycles. *J. Am. Chem. Soc.* **2016**, *138*, 15057−15065.

(17) Ulas, G.; Lemmin, T.; Wu, Y.; Gassner, G. T.; DeGrado, W. F. Designed metalloprotein stabilizes a semiquinone radical. *Nat. Chem.* **2016**, *8*, 354−359.

(18) Yoon, J. H.; Kulesha, A. V.; Lengyel-Zhand, Z.; Volkov, A. N.; Rempillo, J. J.; D'Souza, A.; Costeas, C.; Chester, C.; Caselle, E. R.; Makhlynets, O. V. Uno Ferro, a de Novo designed protein, binds transition metals with high affinity and stabilizes Semiquinone Radical Anion. *Chem.—Eur. J.* **2019**, *25*, 15252−15256.

(19) Tommos, C.; Valentine, K. G.; Martínez-Rivera, M. C.; Liang, L.; Moorman, V. R. Reversible phenol oxidation and reduction in the structurally well-defined 2-mercaptophenol-α_3C protein. *Biochemistry* **2013**, *52*, 1409−1418.
(20) Tommos, C. Insights into the thermodynamics and kinetics of amino-acid radicals in proteins. *Annu. Rev. Biophys.* **2022**, *51*, 453−471.
(21) Finkel, T. Signal transduction by reactive oxygen species. *J. Cell Biol.* **2011**, *194*, 7−15.
(22) Schieber, M.; Chandel, N. S. ROS function in redox signaling and oxidative stress. *Curr. Biol.* **2014**, *24*, 453−462.
(23) Bauer, G.; Speier, G.; Merenyi, G.; Kaizer, J.; Goldstein, S.; Golding, B. T.; Gescheidt, G.; Gebicka, L.; Gebicki, J. L.; Chatgilialoglu, C.; Wardman, P. *Chimia* **2008**, *62*, 704−709.
(24) Wang, C.; Wang, H.; Xu, B.; Liu, H. Oxygen-derived free radicals: Production, biological importance, bioimaging, and analytical detection with responsive luminescent nanoprobes. *View* **2021**, *2*, 20200045.
(25) Sies, H.; Belousov, V. V.; Chandel, N. S.; Davies, M. J.; Jones, D. P.; Mann, G. E.; Murphy, M. P.; Yamamoto, M.; Winterbourn, C. Defining roles of specific reactive oxygen species (ROS) in cell biology and physiology. *Nat. Rev. Mol. Cell Biol.* **2022**, *23*, 499−515.
(26) Cai, J.; Zhu, Y.; Xie, S.; Niu, B.; Zhang, Y.-n.; Li, L.; Li, D.; Zhao, G. Accurate removal of trace 17β-estradiol and estrogenic activity in blended systems under a photoelectrocatalytic circulating flow. *Environ. Sci. Technol.* **2021**, *55*, 12585−12595.
(27) Zhu, P.; Pu, Y.; Wang, M.; Wu, W.; Qin, H.; Shi, J. MnOOH-Catalyzed Autoxidation of Glutathione for Reactive Oxygen Species Production and Nanocatalytic Tumor Innate Immunotherapy. *J. Am. Chem. Soc.* **2023**, *145*, 5803−5815.
(28) Feng, G.; Cheng, P.; Yan, W.; Boronat, M.; Li, X.; Su, J. H.; Wang, J.; Li, Y.; Corma, A.; Xu, R.; Yu, J. Accelerated crystallization of zeolites via hydroxyl free radicals. *Science* **2016**, *351*, 1188−1191.
(29) Dibdin, G. H. E.s.r. of γ-irradiated single crystals of ice at 77 K. Identification of the hydroxyl radical and its trapping site. *Trans. Faraday Soc.* **1967**, *63*, 2098−2111.
(30) Taub, I. A.; Eiben, K. Transient solvated electron, hydroxyl, and hydroperoxy radicals in pulse-irradiated crystalline ice. *J. Chem. Phys.* **1968**, *49*, 2499−2513.
(31) Gligorovski, S.; Strekowski, R.; Barbati, S.; Vione, D. Environmental Implications of Hydroxyl Radicals (•OH). *Chem. Rev.* **2015**, *115*, 13051−13092.
(32) Wang, Z.; Hu, N.; Wang, L.; Zhao, H.; Zhao, G. In Situ Production of Hydroxyl Radicals via Three-Electron Oxygen Reduction: Opportunities for Water Treament. *Angew. Chem., Int. Ed.* **2024**, No. e202407628.
(33) Hou, J.-T.; Zhang, M.; Liu, Y.; Ma, X.; Duan, R.; Cao, X.; Yuan, F.; Liao, Y.-X.; Wang, S.; Ren, W. X. Fluorescent detectors for hydroxyl radical and their applications in bioimaging: A review. *Coord. Chem. Rev.* **2020**, *421*, 213457.
(34) Lottes, B.; Carter, K. P. Capture and stabilization of the hydroxyl radical in a uranyl peroxide cluster. *Chem.—Eur. J.* **2023**, *29*, No. e202300749.
(35) Steiner, T. The Hydrogen Bond in the Solid State. *Angew. Chem., Int. Ed.* **2002**, *41*, 48−76.
(36) Kulshrestha, M.; Ramachandran, C. N.; Gonnade, R. G.; Sadhu, K. K. One pot oxygen mediated syntheses of stable radicals. *Mater. Adv.* **2024**, *5*, 1523−1530.
(37) Mehrgardi, M. A.; Mofidfar, M.; Zare, R. N. Sprayed water microdroplets are able to generate hydrogen peroxide spontaneously. *J. Am. Chem. Soc.* **2022**, *144*, 7606−7609.
(38) Zhu, C.; Francisco, J. S. Production of hydrogen peroxide enabled by microdroplets. *Proc. Natl. Acad. Sci. U. S. A.* **2019**, *116*, 19222−19224.
(39) Niu, B.; Cai, J.; Song, W.; Zhao, G. Intermediate accumulation and toxicity reduction during the selective photoelectrochemical process of atrazine in complex water bodies. *Water Res.* **2021**, *205*, 117663.
(40) Liu, N.; Wang, H.; Wang, S.; Xu, B.; Qu, L. Reactive phosphaphenanthrene aromatic ether diamine endowing epoxy resin with excellent fire resistance, liquid oxygen compatibility and cryogenic mechanical properties. *React. Funct. Poly.* **2023**, *183*, 105500.
(41) Majumdar, A.; Schafer, J.; Mishra, P.; Ghose, D.; Meichsner, J.; Hippler, R. Chemical composition and bond structure of carbon-nitride films deposited by CH4/N2 dielectric barrier discharge. *Surf. Coat. Technol.* **2007**, *201*, 6437−6444.
(42) Herrer, L.; Ismael, A.; Martin, S.; Milan, D. C.; Serrano, J. L.; Nichols, R. J.; Lambert, C.; Cea, P. Single molecule vs. large area design of molecular electronic devices incorporating an efficient 2-aminepyridine double anchoring group. *Nanoscale* **2019**, *11* (34), 15871−15880.
(43) Capitán, M. J.; Álvarez, J.; Navio, C. Study of the electronic structure of electron accepting cyano-films: TCNQ versus TCNE. *Phys. Chem. Chem. Phys.* **2018**, *20*, 10450−10459.
(44) Aarva, A.; Deringer, V. L.; Sainio, S.; Laurila, T.; Caro, M. A. Understanding X-ray spectroscopy of carbonaceous materials by combining experiments, density functional theory and machine learning. part I: fingerprint spectra. *Chem. Mater.* **2019**, *31*, 9243−9255.
(45) Yamakoshi, Y.; Umezawa, N.; Ryu, A.; Arakane, K.; Miyata, N.; Goda, Y.; Masumizu, T.; Nagano, T. Active oxygen species generated from photoexcited fullerene (C_{60}) as potential medicines: $O^{2-\bullet}$ versus $^1O_2$. *J. Am. Chem. Soc.* **2003**, *125*, 12803−12809.
(46) Clément, J. L.; Ferré, N.; Siri, D.; Karoui, H.; Rockenbauer, A.; Tordo, P. Assignment of the EPR Spectrum of 5,5-Dimethyl-1-pyrroline N-Oxide (DMPO) Superoxide Spin Adduct. *J. Org. Chem.* **2005**, *70*, 1198−1203.
(47) Desiraju, G. R. Crystal Engineering: From Molecule to Crystal. *J. Am. Chem. Soc.* **2013**, *135*, 9952−9967.
(48) Mahadevi, A. S.; Sastry, G. N. Cooperativity in Noncovalent Interactions. *Chem. Rev.* **2016**, *116*, 2775−2825.
(49) Vennelakanti, V.; Qi, H. W.; Mehmood, R.; Kulik, H. J. When are two hydrogen bonds better than one? Accurate first-principles models explain the balance of hydrogen bond donors and acceptors found in proteins. *Chem. Sci.* **2021**, *12*, 1147−1162.
(50) Frisch, M. J.; Trucks, G. W.; Schlegel, H. B.; Scuseria, G. E.; Robb, M. A.; Cheeseman, J. R.; Scalmani, G.; Barone, V.; Mennucci, B.; Petersson, G. A.; Nakatsuji, H.; Caricato, M.; Li, X.; Hratchian, H. P.; Izmaylov, A. F.; Bloino, J.; Zheng, G.; Sonnenberg, J. L.; Hada, M.; Ehara, M.; Toyota, K.; Fukuda, R.; Hasegawa, J.; Ishida, M.; Nakajima, T.; Honda, Y.; Kitao, O.; Nakai, H.; Vreven, T.; Montgomery, J. A., Jr.; Peralta, P. E.; Ogliaro, F.; Bearpark, M.; Heyd, J. J.; Brothers, E.; Kudin, K. N.; Staroverov, V. N.; Kobayashi, R.; Normand, J.; Raghavachari, K.; Rendell, A.; Burant, J. C.; Iyengar, S. S.; Tomasi, J.; Cossi, M.; Rega, N.; Millam, N. J.; Klene, M.; Knox, J. E.; Cross, J. B.; Bakken, V.; Adamo, C.; Jaramillo, J.; Gomperts, R.; Stratmann, R. E.; Yazyev, O.; Austin, A. J.; Cammi, R.; Pomelli, C.; Ochterski, J. W.; Martin, R. L.; Morokuma, K.; Zakrzewski, V. G.; Voth, G. A.; Salvador, P.; Dannenberg, J. J.; Dapprich, S.; Daniels, A. D.; Farkas, O.; Ortiz, J. V.; Cioslowski, J.; Fox, D. J. *Gaussian 09*, Revision A.1; Gaussian, Inc., Wallingford, CT, 2009.
(51) Pan, X.; Chen, X.; Li, T.; Li, Y.; Wang, X. Isolation and X-ray Crsytal Structures of Triarylphosphine Radical cations. *J. Am. Chem. Soc.* **2013**, *135*, 3414−3417.
(52) Wen, D.; Li, K.; Deng, R.; Feng, J.; Zhang, H. Defect-Rich Glassy $IrTe_2$ with Dual Enzyme-Mimic Activities for Sono-Photo-synergistic-Enhanced Oncotherapy. *J. Am. Chem. Soc.* **2023**, *145*, 3952−3960.
(53) Lu, T.; Chen, F. Multiwfn: A Multifunctional Wavefunction Analyzer. *J. Comput. Chem.* **2012**, *33*, 580−592.
(54) Sk, M. A.; Kyarikwal, R.; Sadhu, K. K. Remarkable Stability of Glutathione-Based Supramolecular Gel in the Presence of Oxidative Stress from Hydrogen Peroxide. *ACS Appl. Bio Mater.* **2024**, *7*, 6950−6957.

https://doi.org/10.1021/jacsau.4c01115
JACS Au 2025, 5, 61−66